

Proceedings of the ICSC-F'96 Jaszowiec '96

GROWTH, MORPHOLOGY AND SUPERCONDUCTIVITY OF EPITAXIAL $(RE)_1Ba_2Cu_3O_{7-\delta}$ FILMS ON $SrTiO_3$ AND $NdGaO_3$ SUBSTRATES

J.-P. KRUMME, B. DAVID, V. DOORMANN, R. ECKART, G. RABE
AND O. DÖSSEL

Philips GmbH, Forschungslaboratorien, Abteilung Technische Systeme Hamburg
Röntgenstraße 24-26, 22335 Hamburg, Germany

The growth of $(RE)_1Ba_2Cu_3O_{7-\delta}$ (RE: Y, Nd) films on $NdGaO_3$ and $SrTiO_3$ substrates by ion-beam and dc-/rf-magnetron sputter deposition is discussed in the framework of growth kinetics, oxygen exchange, epitaxial relations, substrate crystal orientation, in-plane coherence, vicinal substrate cuts, overgrowth on steps, superconductor/insulator combinations, and patterning by ion-beam etching. The process conditions for ion-beam and magnetron sputter deposition are briefly outlined.

PACS numbers: 74.76.-w, 81.15.-z, 68.65.+g

1. Introduction

The growth of morphologically perfect $(001)(RE)_1Ba_2Cu_3O_{7-\delta}$ (RBCO, RE: Y, Nd) films is still a challenge for technologists due to the anisotropic and complex nature of the crystallographic unit cell of RBCO, its chemical instability in ambient atmosphere, and the lack of proper anisotropic substrate materials. Nevertheless, impressive progress has been made since the advent of this interesting class of superconductors.

This concise article will by far not review all aspects and results published in literature but will rather emphasize the work performed at the Philips Research Lab in Hamburg which was directed towards SQUID applications.

2. Fully coherent epitaxial growth

According to Scheel, the growth regime for step-flow ("layer by layer") of RBCO films is extremely narrow. It requires lattice misfits between film and substrate below 0.1% and very small supersaturation, such as in liquid-phase epitaxy [1]. In contrast, the large supersaturation present in vapor-phase deposition techniques, such as sputtering and chemical vapor deposition (CVD), is

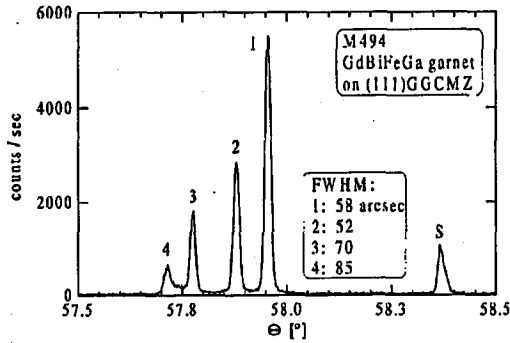


Fig. 1. Symmetric high-resolution X-ray diffractogram (HXRD) of a fully coherent iron-garnet quadrilayer (1-4) on a gallium-garnet substrate (S); on-axis rf-magnetron sputtering: ≈ 1 Pa argon, $\approx 500^\circ\text{C}$, $\approx 1 \mu\text{m/h}$.

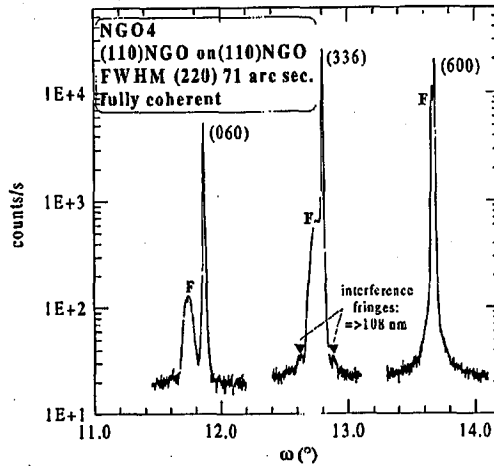


Fig. 2. Asymmetric HXRD of a homoepitaxial fully coherent NdGaO_3 film (F) on a NGO substrate; off-axis rf-magnetron: ≈ 10 Pa Ar/O_2 1:1; 660°C , 30 nm/h; reflection peaks are broadened due to interference, and from the fringe pattern the thickness can be deduced.

expected to result in island formation and step distances much below 100 nm. However, exceptions to this rule are reported for *homoepitaxial* growth. Examples of fully coherent single-crystalline step-free growth are the bismuth-iron garnet films grown in our lab on gallium-garnet substrates. These films are prepared by *on-axis* rf-magnetron sputtering at ≈ 0.5 Pa argon, 500°C , up to 0.3% compressive misfit and rates up to $1 \mu\text{m/h}$ (Fig. 1) [2]. By this technology we have fabricated several- μm thick single-mode low-loss step-index optical waveguides [3]. Furthermore, we have grown fully coherent homoepitaxial SrTiO_3 (STO) and NdGaO_3 (NGO) films by *off-axis* rf-magnetron sputtering at ≈ 10 Pa Ar/O_2 plasma, $\approx 660^\circ\text{C}$ and rates up to 50 nm/h (Fig. 2).

Typically, these films exhibit an expanded a_1 -lattice parameter explained by a population of interstitial ions [4]. All these films feature an extremely small X-ray diffraction line width close to that of the substrate. The fairly low growth temperature and the lack of oxygen added to the sputter gas in the garnet case suggest that the particle energy of condensing species is in a favorable lower range promoting surface diffusion but avoiding damage and resputtering.

3. Crystallography of $(RE)_1Ba_2Cu_3O_{7-\delta}$ compounds

The fairly complex crystallographic unit cell of the compounds RBCO constitutes a layered structure of Cu-O "planes" separated alternately by rare-earth and barium ions (Fig. 3) [5]. Under equilibrium conditions the amount of oxygen deficiency δ can be varied between 1 (tetragonal, semiconducting) and ≈ 0 (orthorhombic, superconducting) by filling the oxygen-lattice sites O(4) and by removing oxygen from the O(5) sites in the Cu-O "chains". The occurrence of su-

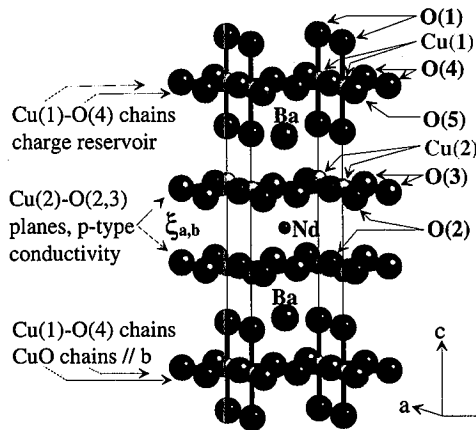


Fig. 3. Crystallographic unit cell of $Nd_1Ba_2Cu_3O_{7-\delta}$.

perconductivity is explained by electron transfer from Cu-O "planes" to O(4) sites leaving p -type conductivity in the Cu-O "planes". Thus, 2-dimensional superconductivity is confined to the (a, b) -plane of RBCO, and (001)-oriented RBCO films are typically favored in device applications [6]. In contrast to yttrium, an excess of neodymium may partially substitute barium, as is expressed by the parameter x in the chemical formula $Nd_{1+x}Ba_{2-x}Cu_3O_{7-\delta}$; increasing x reduces T_c but the structure is more flexible to compensate for non-stoichiometric compositions [7]. The ionic radius of Nd^{3+} (0.108 nm) is between that of Y^{3+} (0.088 nm) and Ba^{2+} (0.129 nm).

4. Plasma processes for $(RE)_1Ba_2Cu_3O_{7-\delta}$ film deposition

For our investigations we have prepared RBCO films by ion-beam sputter epitaxy (IBS) (Fig. 4) and by dc/rf- off-axis magnetron sputter epitaxy (MS).

IBS is reported in detail in Refs. [8, 9]. Briefly, a focused beam of 750 eV Ar^+ or Xe^+ ions is extracted from an rf-excited plasma source, is neutralized by

an electron beam extracted from a dc-discharge, and impinges on a stoichiometric 150 mm diameter RBCO target. At a typical chamber pressure of some 10^{-2} Pa the composition of the sputtered flux condensing on the substrate is deficient in Cu and Ba. Film stoichiometry is established by modulating the sputtered flux by a computer-controlled chopper whose blades coated with Cu and BaO_2 whipe across the beam in vicinity to the target.

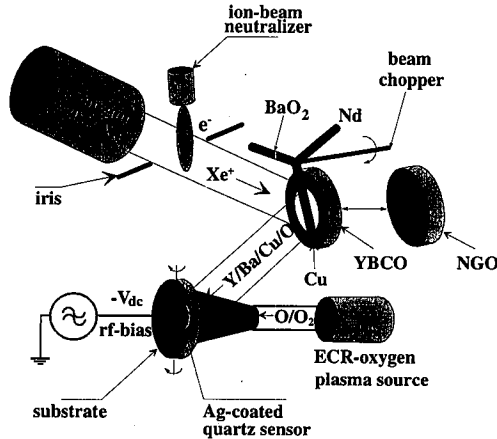


Fig. 4. ECR-oxygen-plasma-assisted ion-beam sputter deposition system: Xe^+ 750 eV 30 mA, 0.05 Pa, e^- 20 eV 40 mA, $10^{16} \text{ O}^-/(\text{cm}^2\text{s})$.

For *in situ* oxidation and phase stabilization the growing film is exposed to an O^-/O stream of $\approx 10^{16}$ atoms/ $(\text{cm}^2 \text{ s})$ from an electron-cyclotron resonance excited (ECR-excited) plasma source [8].

MS of RBCO films is performed in off-axis position in Ar/O_2 plasma at some ten to thirty Pa using a stoichiometric target. Very sensitive process parameters for reaching optimum conditions for low-defect density high- T_c films are the distance to the plasma glow, the total pressure and the Ar/O_2 ratio. We have alternatively used dc- and rf-excitation for RBCO deposition. Two important aspects have to be considered in the sputter deposition of RBCO films, (i) *in situ* oxidation to stabilize the tetragonal phase of RBCO at the growth temperature, and (ii) the protection of the growing film against energetic O^-/O bombardment. As to (i) our growth conditions in IBS and MS range below the tetragonal phase boundary of RBCO, but the presence of atomic oxygen apparently shifts this boundary to considerably lower partial pressures of molecular oxygen. As to (ii) we have investigated the sputter emission of O^- particles from BaO-containing targets by energy-dispersive mass spectrometry [10]. In IBS energetic O^-/O bombardment is circumvented because the target is at floating potential; in contrast, in MS O^- ions are accelerated in the target sheath to the full target potential requiring that the growing film has to be protected by a higher process pressure and/or off-axis position, both being realized in a typical setup as ours. Neutral atomic O species are formed by electron-detachment collisions with gas molecules.

5. Epitaxial growth of $(RE)_1Ba_2Cu_3O_{7-\delta}$ films

5.1. Substrates and surface treatment

Device applications, such as in superconductive quantum-interference devices (SQUIDS), normally require (001) RBCO films of high crystalline perfection. If grain boundaries cannot be avoided — or even be exploited as in step-edge Josephson junctions — they should be well defined. One pre-requisite for this is a very good lattice matching between film and substrate. The most suitable substrate materials so far for $Y_1Ba_2Cu_3O_{7-\delta}$ (YBCO) and $Nd_1Ba_2Cu_3O_{7-\delta}$ (NBCO) films are listed in Table [11–13]. Judging from their temperature dependence the best candidates at the growth temperature for YBCO are NGO and $LaGaO_3$ (LGO) and for NBCO are STO and LGO. A more sophisticated criterion are the similarity in the crystal symmetry and the number of coincident lattice sites. From these the perovskites are the most obvious candidates [14].

Another basic requirement is a high crystalline perfection of the substrate surface. Our cleaning sequence, originally optimized for epitaxial growth of garnets, consists of ultrasound stirring in acetone/propanol, scrubbing by a high-pressure water beam, chemical etching in hot H_3PO_4 , rinsing, scrubbing and centrifuging.

A concise article on interface phenomena of RBCO films is presented in Ref. [15].

TABLE

Substrate	Substrate candidates with perovskite structure.						Therm. exp. coef. [ppm]	ϵ	tan δ (5 GHz 100 K)	Phase trans. [K]	Melting point [K]
	$\Delta a/a$ (300 K) [%]		$\Delta b/b$ (300 K) [%]		$(1/3)\Delta c/c$ (300 K) [%]						
	YBC	NBC	YBC	NBC	YBC	NBC					
$SrTiO_3$	+2.2	+1.1	+0.7	-0.4	+0.3	-0.5	9.4	277	6×10^{-2}	110	2353
$LaAlO_3$	-0.9	-0.2	-2.2	1.1	-3	2.2	10	23	3×10^{-5}	800	2453
$NdGaO_3$	+1	≈ 0	-0.5	-1.6	-0.9	-1.6	11	20	3×10^{-4}	> 1300	1873
YBCO							10–13			≈ 725	≈ 1300

5.2. Process temperature regimes of $Y_1Ba_2Cu_3O_{7-\delta}$ films

The temperature regime for growing RBCO films depends on the epitaxial relations with the substrate material and the deposition process. More specifically, in IBS the different textures of YBCO films form at substrate temperatures which are at least 60 K lower than in MS and crystallize on (100)STO substrates at

temperatures which are at least 40 K lower as compared to (110)NGO substrates. At higher temperatures there is preference for the (001)-texture on (100)STO while the (100)/(010)-texture is preferred on (110)NGO and the (103)/(110)texture on (110)STO and (100)NGO [8, 9].

5.3. c_{\perp} -oriented $Y_1Ba_2Cu_3O_{7-\delta}$ films

The epitaxial relations for (001)YBCO films on different substrates and cuts grown at higher temperatures are depicted in Fig. 5. (001)YBCO films form a mosaic pattern of domains due to an arbitrary alignment of the [100]/[010]YBCO in-plane directions. It appears that the Cu-sublattice couples to the Ti- and Ga-sublattice, respectively. Depending on small variations in total pressure and substrate position the surface morphology of (001)YBCO films, prepared at optimum conditions by off-axis magnetron sputtering, features a minority of out-growths or holes embedded in an orange-peel-like matrix (see Fig. 6); their surface rms-roughness is typically a few nm [9]. On ion-milled STO surfaces (001)YBCO films tend to be even smoother and with fewer precipitates. Precipitates on RBCO films are essentially Cu- or Y-rich [16, 17].

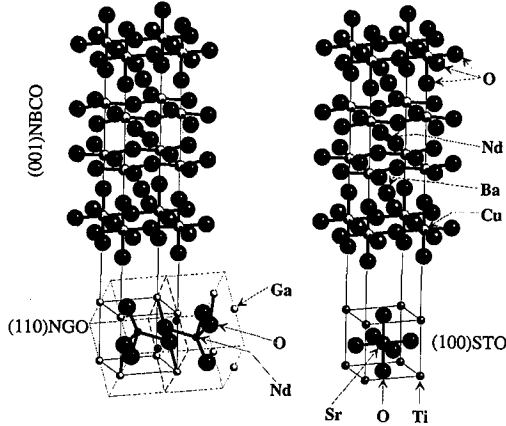


Fig. 5. Epitaxial relations for growth of (001)YBCO films.

5.4. (103)/(110)-oriented $Y_1Ba_2Cu_3O_{7-\delta}$ films

The epitaxial relations for (103)/(110)RBCO films grown on (100)NGO and (110)STO at higher temperature are presented in Fig. 7; from HXRD both textures cannot be discriminated uniquely. Their surfaces represent a groove pattern with triangular cross-section which is aligned parallel to the [001]_S substrate direction of NGO and STO. Parallel to [001]_S the X-ray diffraction line width is extremely narrow associated with excellent superconductivity; along the orthogonal in-plane directions [010]_{NGO} and $[-110]$ _{STO} the electrical resistivity and HXRD line width are significantly higher [9].

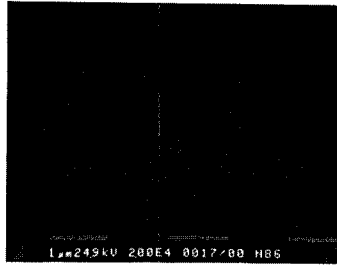


Fig. 6. Scanning-electron micrograph (SEM) of a (001)YBCO film on (100)STO by dc-off-axis MS: 16 Pa Ar/O₂ 2:1, 775°C.

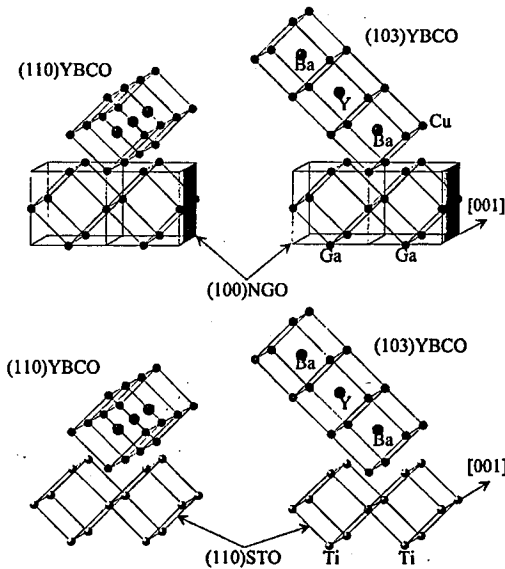


Fig. 7. Epitaxial relations for growth of (103)/(110)YBCO films.

5.5. $(a, b)_{\perp}$ -oriented $Y_1Ba_2Cu_3O_{7-\delta}$ films

The epitaxial relations for (100)/(010)YBCO films grown at medium deposition temperatures are shown in Fig. 8. Similar to (001)YBCO films, a mosaic pattern of domains is formed on (100)STO due to non-preferential alignment of the [001]YBCO direction [18]. Full in-plane coherence may be realized for (100)/(010)YBCO films on (110)NGO by ordering the [001]YBCO axis parallel and normal to the [001]NGO axis, associated with an rms-roughness of ≈ 1 nm [9]. In the special case of (100)SrLaGaO₄ substrates a uniform alignment of the [001]YBCO axis along the [001]SrLaGaO₄ axis has been reported. This is explained by sub-nanometer grooves formed by oxygen octahedra in the (100)SrLaGaO₄ surface, which provide preferential nucleation sites for YBCO [19].

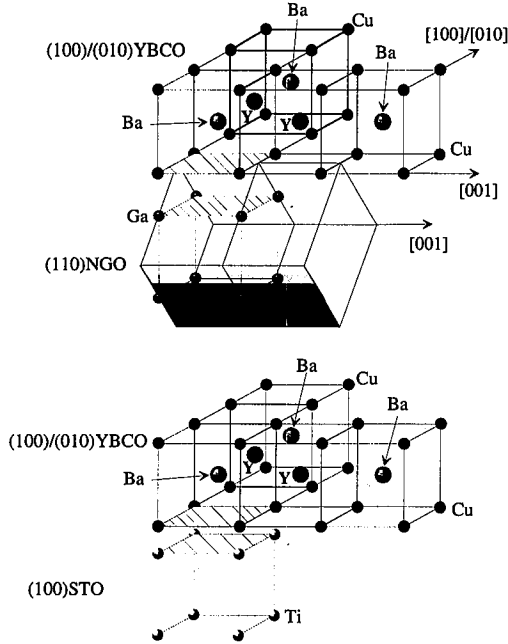


Fig. 8. Epitaxial relations for growth of (100)/(010)YBCO films.

This “grapho-epitaxial” situation is somewhat similar to the in-plane aligned growth of the [001]YBCO axis on (100)NGO and (110)STO surfaces (Sec. 5.4).

5.6. Quasi-cubic semiconducting YBaCuO films

At lower growth temperature the fully in-plane coherent, quasi-cubic and semiconducting YBCO films exhibit extremely low X-ray diffraction line width (Fig. 9) and sub-nanometer rms-roughness [9].

5.7. c_{\perp} -oriented $Nd_1Ba_2Cu_3O_{7-\delta}$ films

(001)NBCO films crystallize fully coherently on (100)STO (Fig. 10) but typically exhibit a minority population of (100)/(010)NBCO grains even at a fairly high growth temperature. They have excellent superconducting properties with $T_c > 91$ K and $R_{300}/R_{100} \approx 3$ and sub-nanometer surface rms-roughness [20].

A bilayer composed of a ≈ 100 nm thick (100)STO film on a ≈ 100 nm thick (001)NBCO film grown on a (100)STO substrate features nearly full in-plane coherence to the underlying NBCO film concomitant with an extremely small X-ray diffraction line width of both films (Fig. 11).

The buried NBCO film exhibits tetragonal symmetry and expanded lattice parameter c_{\perp} due to an oxygen deficiency $\delta > 0.45$; this suggests that the STO film on top constitutes a dense barrier to oxygen diffusion so that the tetragonal-to-orthorhombic phase transition of the buried NBCO film during cool-down could not occur. The oxygen diffusivity in STO compares with the slow

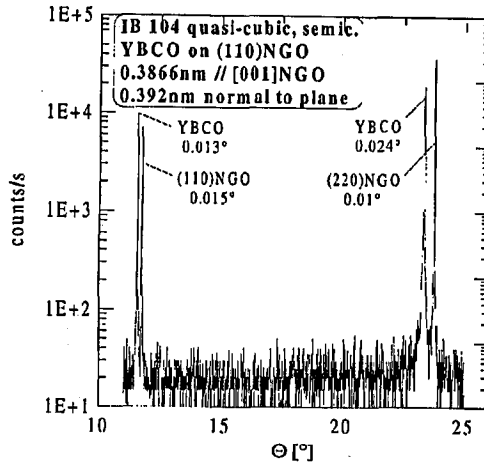


Fig. 9. Symmetric HXRD of a semiconducting quasi-cubic YBCO film on (110)NGO by IBS: 615°C, 1 μm thick.

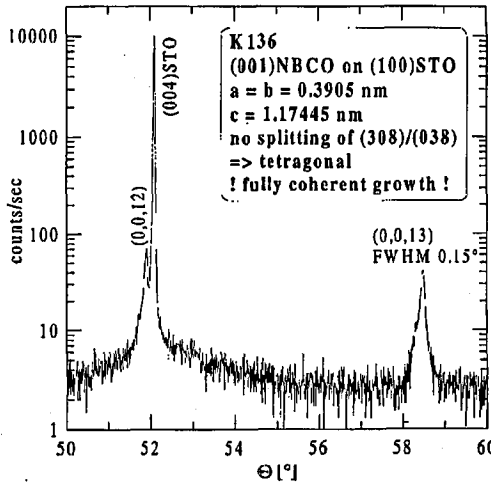


Fig. 10. Symmetric HXRD of a (001) $\text{Nd}_1\text{Ba}_2\text{Cu}_3\text{O}_{7-\delta}$ films on (100)STO by off-axis rf-MS: 825°C.

diffusion rate along the [001]YBCO direction; in contrast, NGO exhibits an oxygen diffusivity similar to the (001)YBCO plane [21]. While annealing of as-grown films in molecular oxygen at 400°C does not reduce the c_{\perp} -parameter, the superconductivity in 10 μm wide microbridges which were ion-beam etched from this STO/NBCO bilayer could be recovered by annealing. In contrast, atomic oxygen may penetrate a capping layer of NGO efficiently at 540°C to saturate the underlying (001)YBCO film [22].

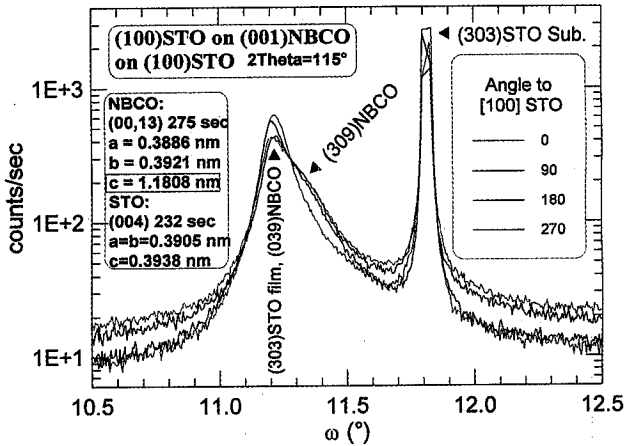


Fig. 11. Asymmetric HXRD of a coherently epitaxial bilayer (100)STO/(001)NBCO/(100)STO substrate by off-axis rf-MS.

6. Further device-relevant aspects in the sputter epitaxy of $(RE)_1Ba_2Cu_3O_{7-\delta}$ films

6.1. Full or partial in-plane coherence of epitaxial $(RE)_1Ba_2Cu_3O_{7-\delta}$ films

Depending on the crystallographic status of the substrate surface and the lattice-misfit conditions RBCO films either crystallize *fully* coherently at the substrate interface, i.e. continue to grow with the same in-plane parameters and orientation of their lattice as those of the substrate. Or, epitaxial RBCO films may rather align with their lattice normal to the interface and parallel to the major in-plane axes of the substrate; the formation of misfit dislocations results in relaxed lattice constants in the film [23]. The latter case is more abundant at higher deposition temperatures and is called *partial* coherence. Partial coherence is evident in samples grown on miscut substrates by an uncorrelated shift of the diffraction peaks of film and substrate upon azimuth rotation.

Both cases are illustrated in Fig. 12 by HXRD rocking curves. Evidently, our chemical-etching procedure promotes fully coherent epitaxy under otherwise optimized conditions.

6.2. Growth of $(RE)_1Ba_2Cu_3O_{7-\delta}$ films on vicinal substrates

Normally, the specified crystallographic orientation of the substrate surface deviates by some tenth of a degree from the nominal orientation, which is called a miscut. As treated in Ref. [24] for the case of a nominal (100)LaAlO₃ substrate with miscut δ , unit-cell high parallel ledges of width λ develop with (100)LaAlO₃ facets. These steps provide aligned and enhanced nucleation sites for RBCO. If the ledge width λ is larger than the diffusion length λ_d of adatoms of RBCO, then, island growth dominates concomitant with the typical granular orange-peel morphology [23]. At larger miscut angles δ we have $\lambda_d > \lambda$; then, step-flow prevails

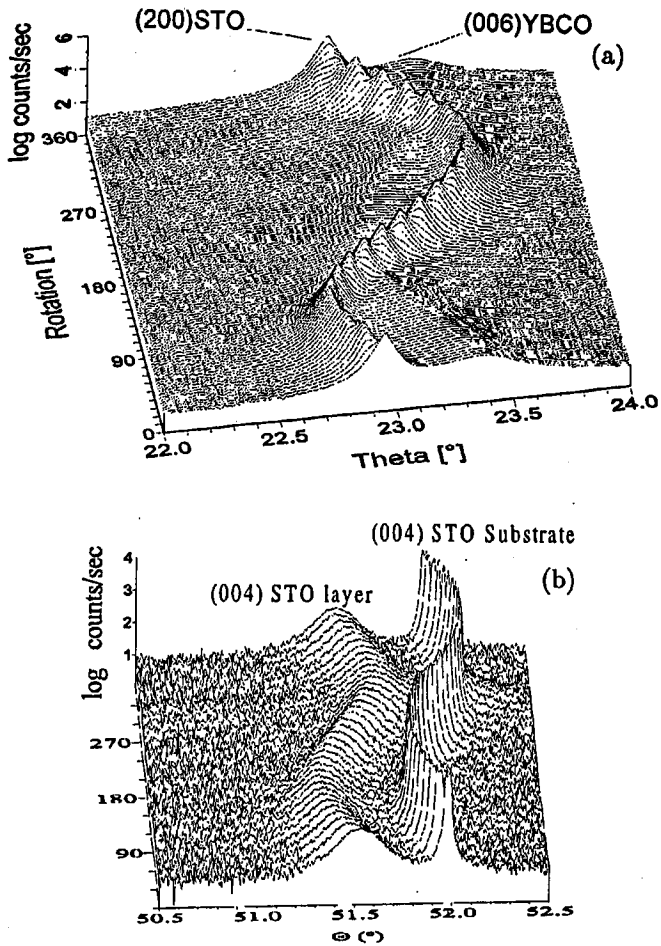


Fig. 12. Symmetric IXRD rocking curves of (a) an incoherent (001)YBCO film on (100)STO and (b) a fully coherent (100)STO film on (100)STO; in (a) the substrate is unetched, in (b) the substrate is etched in hot phosphoric acid.

which results in a reduced number of outgrowths and growth spirals (dislocations), an elongated grain structure, higher T_c values, and anisotropic j_c relative to the ledges. The value of λ_d depends on the energy of the condensing adatoms and may be altered by plasma interactions. This may be one reason for the low deposition temperature of garnet films grown by *on-axis* rf-MS at low argon pressure and substrate temperatures (see Fig. 1).

6.3. Epitaxial growth of STO and NGO on unit-cell steps of $(RE)_1Ba_2Cu_3O_{7-\delta}$

For device elements to be used in SQUIDS, such as ramp-type Josephson tunnel junctions, conductor crossovers, contact windows and magnetometer coils, a multilayer technology combining RBCO and insulator films had to be developed which masters the specific problem of step coverage. For coherent growth the slopes

have to be small ($< 20^\circ$ from in-plane). A good lattice match at unit-cell steps of (001)YBCO is established by stacks of three unit cells of either (100)STO or (110)NGO.

We have prepared SQUIDs by IBS featuring ramp-type Josephson junctions with a nominally 2 nm thick NGO barrier. Their excellent Josephson properties, relatively high electrical resistance, and their nm-smooth surface suggest that this ultrathin NGO barrier and the upper YBCO film grow coherently on the ramped lower YBCO film [25].

6.4. Diffusivity of oxygen in the (a, b) -plane of $\text{Nd}_1\text{Ba}_2\text{Cu}_3\text{O}_{7-\delta}$

Apart from the 2-dimensional superconductivity confined between the CuO_2 -“planes” (see Fig. 3) the layered structure of the unit cell of $(\text{RE})_1\text{Ba}_2\text{Cu}_3\text{O}_{7-\delta}$ promotes oxygen diffusion along the (100)/(010)RBCO plane. Patterning of microbridges by ion-beam etching results in loss of superconductivity if RBCO films are not cooled [20]. We have found that this process is particularly pronounced in (001)NBCO on (100)STO, as compared to (001)YBCO on (100)STO, but degradation of T_c can be widely suppressed if the NBCO film is cooled to very low

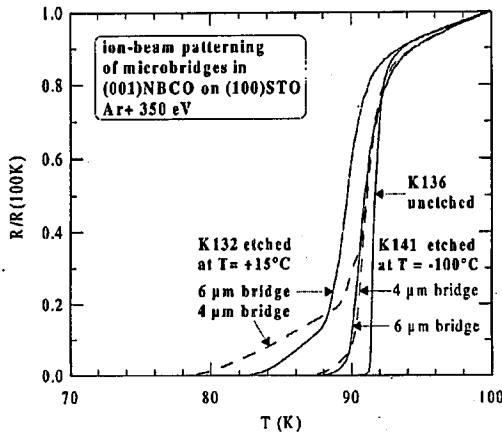


Fig. 13. Resistance R vs. temperature T dependence of microbridges in (001)NBCO films in comparison to the typical unpatterned (001)NBCO film K136; patterning by ion-beam etching at 350 eV Ar^+ cooled by water or liquid N_2 .

temperatures, as shown in Fig. 13. We propose that this deterioration results from oxygen out-diffusion facilitated by the homogeneous grain-boundary structure in these sub-nm smooth NBCO films. Also, the effect of oxygen deficiency δ on the superconductivity in NBCO is more pronounced than in YBCO [26].

6.5. Grain boundaries and interfaces in $\text{Y}_1\text{Ba}_2\text{Cu}_3\text{O}_{7-\delta}$ films

The performance of devices such as SQUIDs is strongly influenced by grain boundaries and interfaces. Grain boundaries [27] are exploited as barriers in step-edge Josephson junctions, and interfaces play a role in ramped Josephson junctions with ultrathin artificial tunnel barriers [25, 28]. YBCO films grow on

$\approx 80^\circ$ -steep steps in the (100)STO substrate by forming a_\perp -grains with 90° -basal-plane-faced and 90° -symmetrical-tilt grain boundaries adjacent to c_\perp -grains at the rim. However, this grain-boundary structure is not yet reproducible enough for commercialization of SQUIDs with step-edge Josephson junctions. However, in bicrystal grain-boundary junctions the grain-boundary structure can be mastered satisfactorily.

The control of barriers is still an issue for research since Josephson effects depend critically on interface phenomena.

7. Conclusion

Roughly a decade has elapsed since the advent of the first high- T_c superconductor and, since then, substantial progress has been made in mastering the technology. The results so far confirm that coherent, epitaxial crystallization of $(RE)_1\text{Ba}_2\text{Cu}_3\text{O}_{7-\delta}$ films on NdGaO_3 , SrTiO_3 and similar substrates is governed by the same rules as in classical semiconductor technology but the narrow constraints for single-crystalline coherent epitaxial growth are not yet fulfilled. There is much room for further improvements before reliable electronic devices will gain a sizeable market share. Specifically, in SQUIDs the technology for artificial barriers needs further efforts.

Acknowledgment

It is acknowledged that, in particular, the groups of S. Miyazawa/NTT Laboratories and T. Morishita/SRL-ISTEC have contributed to the understanding of RBCO growth.

This work has been partly sponsored by the German Ministry of Education and Sciences.

References

- [1] H.J. Scheel, *MRS Bull.* **19**, 26 (1994); H.J. Scheel, C. Klemenz, F.K. Reinhart, H.P. Lang, H.J. Güntherodt, *Appl. Phys. Lett.* **65**, 901 (1994).
- [2] J.-P. Krumme, V. Doormann, P. Hansen, H. Baumgart, J. Petruzzello, M.P.A. Viegars, *J. Appl. Phys.* **66**, 4393 (1989).
- [3] J.-P. Krumme, V. Doormann, H. Meyer, W. Radtke, B. Strocka, *SPIE Proc.* **1018**, 109 (1988).
- [4] E.J. Tarsa, E.A. Hachfeld, F.T. Quinlan, J.S. Speck, M. Eddy, *Appl. Phys. Lett.* **68**, 490 (1996).
- [5] H. Shaked, B.W. Veal, J. Faber, R.L. Hitterman, U. Balachandrian, G. Tomlins, H. Shi, L. Morss, A.P. Paulikas, *Phys. Rev.* **41**, 4173 (1990).
- [6] M. Cyrot, D. Pavuna, *Introduction to Superconductivity and High- T_c Materials*, World Scientific, Singapore 1992.
- [7] M. Badaye, F. Wang, Y. Kanke, K. Fukushima, T. Morishita, *Appl. Phys. Lett.* **66**, 2131 (1995).
- [8] J.-P. Krumme, V. Doormann, F. Welz, O. Dössel, H. van Hal, *J. Mater. Res.* **9**, 2747 (1994).
- [9] J.-P. Krumme, V. Doormann, F. Welz, R. Eckart, O. Dössel, W. Dingen, K. Schiffmann, *J. Mater. Res.* **9**, 3032 (1994).

- [10] J.-P. Krumme, R.A.A. Hack, I.J.M.M. Raaijmakers, *J. Appl. Phys.* **70**, 6743 (1991).
- [11] M. Sasaura, S. Miyazawa, M. Mukaida, *J. Appl. Phys.* **68**, 3643 (1990).
- [12] E.A. Giess, R.L. Sandstrom, W.J. Gallagher, A. Gupta, S.L. Shinde, R.F. Cook, E.I. Cooper, E.J.M. O'Sullivan, J.M. Roldan, A.P. Seegmüller, J. Angilello, *IBM J. Res. Dev.* **34**, 916 (1990).
- [13] J.M. Phillips, *J. Appl. Phys.* **79**, 1829 (1996).
- [14] R. Guo, A.S. Bhalla, L.E. Cross, R. Roy, *J. Mater. Res.* **9**, 1644 (1994).
- [15] M. Kawasaki, M. Nantoh, *MRS Bull.* **19**, 33 (1994).
- [16] Z. Han, T.I. Selinder, U. Helmerson, *J. Appl. Phys.* **75**, 2020 (1994).
- [17] J.-P. Locquet, Y. Jaccard, C. Gerber, E. Mächler, *Appl. Phys. Lett.* **63**, 1426 (1993).
- [18] C.B. Eom, A.F. Marshall, S.S. Laderman, R.D. Jacowitz, T.H. Geballe, *Science* **249**, 1549 (1990).
- [19] S. Miyazawa, M. Mukaida, *Appl. Phys. Lett.* **64**, 2160 (1994).
- [20] B. David, S. Krey, R. Eckart, V. Doormann, G. Rabe, J.-P. Krumme, O. Dössel, *IEEE Trans. Appl. Supercond.* **7** (1997).
- [21] S.C. Tidrow, W.D. Wilber, A. Tauber, S.N. Schauer, D.W. Eckart, R.D. Finnegan, R.L. Pfeffer, *J. Mater. Res.* **10**, 1622 (1995).
- [22] G. Ockenfuß, R. Wördenweber, T.A. Scherer, R. Unger, W. Jutzi, *Physica C* **241**, 24 (1995).
- [23] D.G. Schlom, D. Anselmetti, J.G. Bednorz, R.F. Broom, A. Catana, T. Frey, Ch. Gerber, H.J. Güntherodt, H.P. Lang, J. Mannhart, *Z. Phys. B, Condens. Matter* **86**, 163 (1992).
- [24] R.R. Biggers, M.G. Norton, I. Maartense, T.L. Peterson, E.K. Moser, D. Dempsey, M.A. Capano, J. Talvacchio, J.L. Brown, J.D. Wolf, *IEEE Trans. Appl. Supercond.* **5**, 1241 (1995).
- [25] D. Grundler, J.-P. Krumme, B. David, O. Dössel, *Appl. Phys. Lett.* **65**, 1841 (1994).
- [26] T. Nishimura, Y. Kido, M. Badaye, Y. Yoshida, F. Wang, T. Morishita, M. Kumagai, *J. Appl. Phys.* **79**, 14 (1996).
- [27] S.E. Babcock, *MRS Bull.* **17**, 20 (1992).
- [28] K. Char, *MRS Bull.* **19**, 51 (1994).